Single-particle kinetics of influenza virus membrane fusion

Floyd, Daniel L.; Ragains, Justin R.; Skehel, John J.; Harrison, Stephen C.; Oijen, Antoine M. van

Published in:
Proceedings of the National Academy of Sciences of the United States of America

DOI:
10.1073/pnas.0807771105

Publication date:
2008

Supporting Information

Floyd *et al.* 10.1073/pnas.0807771105

SI Methods

Surface Functionalization. ***Cleaning.*** Glass microscope coverslips (25 × 25 mm; No. 1.5; VWR Scientific) were cleaned in a bath sonicator while immersed successively in detergent, 1 M potassium hydroxide, ethanol, and acetone. All solvents used in surface cleaning and functionalization were HPLC grade. The coverslips were then submerged in a 3:1 solution of sulfuric acid and 30% hydrogen peroxide for 15 min. This final cleaning step served to remove any remaining organic residue from the glass and leave a uniform hydrophilic surface. After a final water rinse, the coverslips were dried in a laboratory oven for 1 h at 120°C.

Silane and dextran deposition. Cleaned microscope cover slips were agitated for 5 min in a 0.2% (vol/vol) solution of (3-glycidooxypropyl)trimethoxysilane in isopropanol followed by rinsing in additional isopropanol to remove excess silane. The adsorbed silane layer was cured for 1 h at 80°C. Dextran 500 (GE Healthcare; mean molecular weight, 5×10^5) was dissolved in deionized water to make a 30% solution (3 g/10 ml), and the silanized coverslips, arranged on a flat surface, were covered with ≈1 ml of this solution. The reaction was left undisturbed for 24–36 h. Unreacted dextran was removed by soaking the coverslips for 48 h in deionized water. Finally, the dextran-functionalized coverslips were dried in an oven at 80°C and stored in a vacuum desiccator.

Microfluidic Flow-Cell Fabrication. Flow-cell channels were constructed by cutting a 15 × 2-mm channel into a 20 × 20-mm piece of double-stick tape (Grace Bio-Labs). The tape was then sandwiched between a dextran functionalized coverslip and a 20 × 20 × 1-mm fused quartz microscope slide with holes drilled at either end of the channel. Twenty-centimeter lengths of polyethylene tubing (Intramedic; I.D. = 0.38 mm) were inserted into these holes, and the flow-cell was sealed with epoxy glue.

Supported Bilayer Preparation. Liposomes were composed of a 4:4:2:0.1:5×10^{-5} ratio of 1,2,dioleoyl-*sn*-glycero-3-phosphocholine (DOPC) (Avanti Polar Lipids), 1-oleoyl-2-palmitoyl-*sn*-glycero-3-phosphocholine (POPC) (Avanti Polar Lipids), cholesterol (Avanti Polar Lipids), bovine brain disialoganglioside GD_{1a} (Sigma), and *N*-((6-(biotinoyl)amino)hexanoyl)-1,2-dihexadecanoyl-*sn*-glycero-3-phosphoethanolamine (biotin-X DHPE) (Molecular Probes). Lipids were mixed in a test tube as chloroform/methanol solutions, and the solvent was removed by evaporation under a stream of argon or nitrogen gas. Residual solvent was removed from the lipid film by placing the test tube in a vacuum desiccator for at least 2 h. The dried lipid film was then suspended by gentle agitation in HNE (5 mM Hepes, 145 mM NaCl, 0.2 mM EDTA) buffer at a concentration of ≈10 g/liter, and liposomes were extruded through a polycarbonate membrane filter with pore sizes of 100 nm. Liposomes were drawn into the flow cell and incubated for 30 min. During this time liposomes adsorbed to the surface, fused with neighboring liposomes until they ruptured and spread over the surface to form a lipid bilayer.

Preparation of Rhodamine 110 Octadecyl Ester Trifluoroacetate Salt. A mixture of 30 mg (0.08 mmol) of rhodamine 110 chloride salt and 7.5 g of octadecanol under argon was warmed in a preheated oil bath at 80°C until complete melting of the octadecanol was observed. Concentrated sulfuric acid (0.1 ml) was then added, and the reaction mixture was allowed to stir for 48 h after which 0.6 ml of dry triethylamine was added dropwise over the course of 5 min. Upon completion of triethylamine addition, the reaction mixture was allowed to cool to 25°C. The resulting solid was suspended in 100 ml of diethyl ether and stirred vigorously for 40 min. Filtration of the resulting suspension afforded ≈1.5 g of a bright red solid that was subjected to column chromatography. To a column with a diameter of 3 cm was added a slurry of 2 g of silica gel in 10% isopropanol in chloroform. The silica plug was then topped off with a slurry of 20 g of neutral alumina in 10% isopropanol in chloroform. The compound was eluted with 100 ml each of 10%, 20%, 30%, and 40% isopropanol in chloroform followed by 300 ml of 10% methanol plus 20% isopropanol in chloroform. Evaporation of UV-active fractions afforded 33 mg of a bright red solid that was further subjected to HPLC (10 ml/min on a C4 prep. column; 10 min at 10% isopropanol and 0.1% TFA in water followed by a 45-min ramp to 90% isopropanol and 0.1% TFA in water). The resulting solid was washed with 20 ml of ether to afford 28 mg (50%) of a red solid. 1H NMR (600 MHz, CD3OD): δ 8.30 (d, 1H, J = 7.8 Hz); 7.85 (dt, 1H, J = 7.8 Hz, J = 1.8 Hz); 7.81 (dt, 1H, J = 7.8 Hz, J = 1.8 Hz); 7.42 (d, 1H, J = 7.2 Hz); 7.06 (d, 2H, J = 9.0 Hz); 6.81–6.84 (m, 4H); 3.94 (t, 2H, J = 6.3 Hz); 1.22–1.33 (m, 28H); 1.13 (m, 4H); 0.94 (m, 2H); 0.90 (t, 3H, J = 7.2 Hz). 13C NMR (150 MHz, CD3OD): 165.7; 160.2; 160.1; 158.5; 133.4; 132.7; 131.7; 131.1; 130.7; 130.3; 116.8; 113.8; 97.3; 65.6; 31.9; 29.6; 29.54; 29.51; 29.48; 29.30; 29.26; 29.1; 28.2; 25.8; 22.2; 13.2. HRMS calculated for C_{38} $H_{51}N_2O_3$ (M+): 583.3900; found 583.3906.

Labeling and Purification of Viral Particles. Influenza particles were labeled with sulforhodamine B (SRB) (Aldrich) and rhodamine 110 octadecyl ester (Rh110C18). Ten microliters of influenza virus (≈10 μg of viral protein) were mixed with 20 μl of 20 mM SRB in HNE buffer and left at room temperature for 16–20 h. Unincorporated dye was separated from the virus with a gel-filtration column (PD-10 desalting column; GE Healthcare) in a total volume of 0.8 ml. A 2 mM solution of Rh110C18 was prepared in dimethylformamide, and 13 μl was added to the SRB-labeled virus particles and agitated for 3 h. A second PD-10 column was used to separate the virus from free Rh110C18. Both dyes remained stably associated with the virus for several hours.

Microscope Configuration. Single-particle fusion assays were conducted on an inverted fluorescence microscope (Nikon TE-2000U) with a high numerical aperture objective (N.A. = 1.45). Viral particles were illuminated with an argon/krypton laser (Coherent Innova 70C) operating in the multiline mode. The "white" beam emitted from the laser was dispersed with a series of two equilateral prisms. The separated 488- and 568-nm lines were band-pass-filtered (Chroma Technology) and combined with a dichroic mirror before being focused on the outer edge of the objective back focal plane. Fluorescence emission was collected with the objective and filtered through a 500- to 540-nm and 600- to 640-nm dual band-pass emission filter (Chroma Technology). Outside of the microscope, the emission light was collimated and split into separate green and red channels by using another dichroic mirror, and each channel was focused onto separate regions of an electron multiplying CCD camera (Andor Technology DV 887-BI).

Execution of the Fusion Assay. A flow cell with a prepared supported membrane was mounted on the microscope stage and

coupled to a peristaltic pump (VWR Scientific) calibrated to draw buffer at a rate of ≈0.1 ml/min. Labeled virus was diluted to ≈50 ng/ml and pumped into the flow cell until the surface was saturated or the desired particle density had been reached. Fluorescein-labeled streptavidin (Molecular Probes) was diluted to 2 μg/ml in HNE buffer and then pumped into the flow cell for 2 min followed by a 1-min wash with HNE buffer. The fusion reaction was then initiated by flowing an acidic buffer containing 10 mM citric or acetic acid, 140 mM NaCl, 0.1 mM EDTA, and 0.01% NaN_3. Time-lapsed fluorescence images were recorded at 10 Hz for 200–400 s by using Andor iQ imaging software.

Data Analysis. ***Particle detection and fluorescence intensity extraction.*** Ten images acquired before onset of fusion were averaged and band-pass-filtered to remove noise and background intensity. Particles were located by calculating the center-of-mass positions of fluorescent regions. To identify red and green fluorescence intensities corresponding to individual viral particles, the image was divided into red and green channels and the 2D cross-correlation function was calculated. The offset coordinates corresponding to the maximum correlation was then used to match the red and green intensities of each particle. Fluorescence trajectories were from calculated by integrating the intensities from a 4 × 4-pixel region around each particle. All data were analyzed with software written in MATLAB.

pH sensor. The background intensity of the green channel was integrated to measure the emission from the fluorescein-streptavidin pH sensor. When acidic buffer reached the membrane surface, the fluorescence quantum yield of the surface bound fluorescein significantly decreased and resulted in a drop in fluorescence. The time of the pH drop was estimated from the integrated fluorescence trajectory by finding the intersection of a best-fit line through the base-line and the tangent-line passing through the point with the minimum slope.

Fusion event detection. Trajectories were plotted and manually selected for particles showing fusion activity. Hemifusion and pore formation were defined as the maximum rates of fluorescence increase or decay. To facilitate event detection, each trajectory was transformed by using a first-order Savitzky-Golay differentiation filter. The maximum or minimum values of the resulting time-derivative traces yielded the respective hemifusion and pore-formation times. Event times were recorded and plotted as hemifusion and pore formation probability distribution histograms. Additionally, the lag time between hemifusion and pore formation was calculated for each viral particle and plotted.

Kinetic Analysis. Multiexponential fusion kinetics arise from a reaction scheme in which the virus passes through N sequential steps before hemifusion:

$$A \xrightarrow{k_1} X_1 \xrightarrow{k_1} X_2 \rightarrow \xrightarrow{k_1} X_{N-1} \xrightarrow{k_1} H. \qquad [1]$$

Each transition is a random (Poisson) process, and the probability of turnover at time t is $k_1 \cdot \exp(-k_1 t)$. The overall hemifusion probability density function consists of the convolution of each intermediate step. Since convolution is equivalent to multiplication in the frequency domain, we make use of the Laplace transform:

$$\tilde{P}(s) = \int_0^\infty p(t) e^{-st}\, dt = \frac{k_1}{s + k_1}, \qquad [2]$$

where s is the Laplace variable (1). The transformed hemifusion probability density function is then the product of each step:

$$\tilde{P}_H(s) = \left(\frac{k_1}{s + k_1}\right)^N. \qquad [3]$$

Finally, we obtain the hemifusion probability density function by transforming back to the time domain:

$$p_H(t) = \frac{1}{2\pi i} \int_0^{i\infty} \tilde{P}_H(s) e^{st}\, ds = \frac{k_1^N\, t^{N-1}}{\Gamma(N)} e^{-k_1 t}. \qquad [4]$$

The transition from the hemifusion intermediate to pore formation is modeled as a single exponential decay:

$$P_{H \rightarrow P}(t) = k_2 e^{-k_2 t}. \qquad [5]$$

The overall lag-time from pH drop to pore formation is a convolution of the hemifusion lag time and the hemifusion lifetime distributions (or a linear combination in the Laplace domain):

$$\begin{aligned} P_P(t) &= \frac{1}{2\pi i} \int_0^{i\infty} \tilde{P}_H(s) \tilde{P}_{H \rightarrow P}(s) e^{st} ds \\ &= \frac{k_2 k_1^N}{(k_1 - k_2)^N} \frac{\Gamma(N, (k_1 - k_2)t)}{\Gamma(N)} e^{-k_2 t}, \end{aligned} \qquad [6]$$

where

$$\tilde{P}_{H \rightarrow P}(s) = \frac{k_2}{s + k_2}, \qquad [7]$$

$$\Gamma(N) = \int_0^\infty t^{N-1} e^t dt, \qquad [8]$$

and

$$\Gamma(N, (k_1 - k_2)t) = \int_0^{(k_1 - k_2)t} t^{N-1} e^t\, dt \qquad [9]$$

are the gamma and lower incomplete gamma functions, respectively.

A very similar kinetic description can be applied to a reaction scheme in which N parallel and stochastic steps must take place before hemifusion:

$$\begin{array}{l} A_1 \overset{k_1}{\searrow} \\ A_2 \overset{k_1}{\rightarrow} H \overset{k_2}{\rightarrow} P \cdot \\ A_N \overset{k_1}{\nearrow} \end{array} \qquad [10]$$

Although each step occurs independently, the resulting hemifusion lag-time distribution will show the same rise and decay pattern that results from a sequential chain of stochastic events. This result can be explained by recalling that an exponentially distributed Poisson process has no memory. Suppose that the first event in the parallel scheme occurs by chance at time t. The probability that the second step will occur at some later time, $t + \tau$, is also an exponential distribution from time t. Consequently, the probability distribution of the second event is the convolution of both distributions. Just as in the sequential model, the hemifusion lag-time distribution can be derived from the convolution of each of the required N kinetic steps, resulting in

a gamma distribution. As described in the main text, we interpret this parallel model as corresponding to the rate-limited conformational transition of hemagglutinin trimers after proton activation. Any of the HA's located within the contact area could contribute to the fusion process, so in our model, the rate constant k_1 is proportional to the number of proteins available to participate in each of the N required transitions. This number depends on the size of the contact area but is likely to be significantly larger than N. Therefore, each intermediate transition would occur with the same rate on average, allowing our kinetic data to be fitted with a gamma distribution. The fusion rate constants were estimated by minimizing the error of N, k_1, and k_2, (Eqs. **5** and **6**) against the experimental time distributions, using a nonlinear least-squares fitting algorithm in MATLAB or OriginLab. For more details and background, see refs. 2 and 3.

1. Carrier GF, Krook M, Pearson CF (1983) *Functions of a Complex Variable* (Hod Books, Ithaca).
2. Feller W (1968) *An Introduction to Probability Theory and Its Applications* (Wiley, New York).
3. Schnitzer MJ, Block SM (1995) *Cold Spring Harb Symp Quant Biol* 60:793–802.

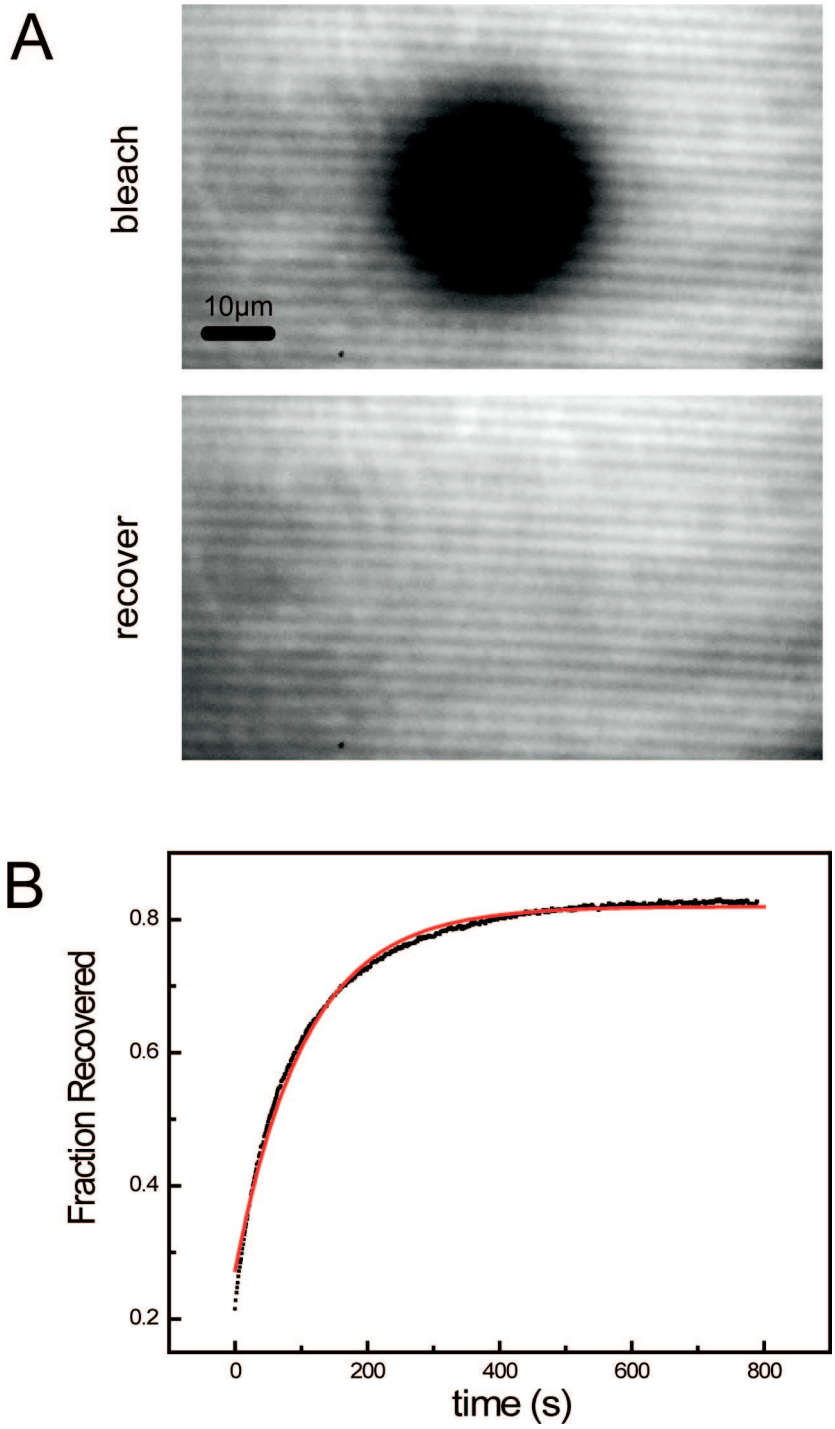

Fig. S1. Measurement of membrane fluidity measured by fluorescence recovery of photobleaching. (*A*) Circular area of a tetramethylrhodamine-labeled bilayer photobleached with a high-intensity (≈250 W·cm^{-2}), 568-nm laser, and recovery observed under low-intensity excitation. (*B*) Normalized fluorescence trajectory of the photobleached area. The lipid diffusion coefficient (*D*) was estimated as described by Axelrod *et al.* (*Biophys J* 16:1055–1069) where $D = 0.22R^2/t$ and *R* is the radius of the circular photobleached area. The half recovery time (*t*) was obtained by fitting the data to the expression, $y = A(1 - 2^{(-x/t)})$. The best-fit recovery half-time is $t = 73.6 \pm 0.4$ s and $D = 0.747 \pm 0.004$ μm^2·s^{-1}, consistent with a fluid bilayer.

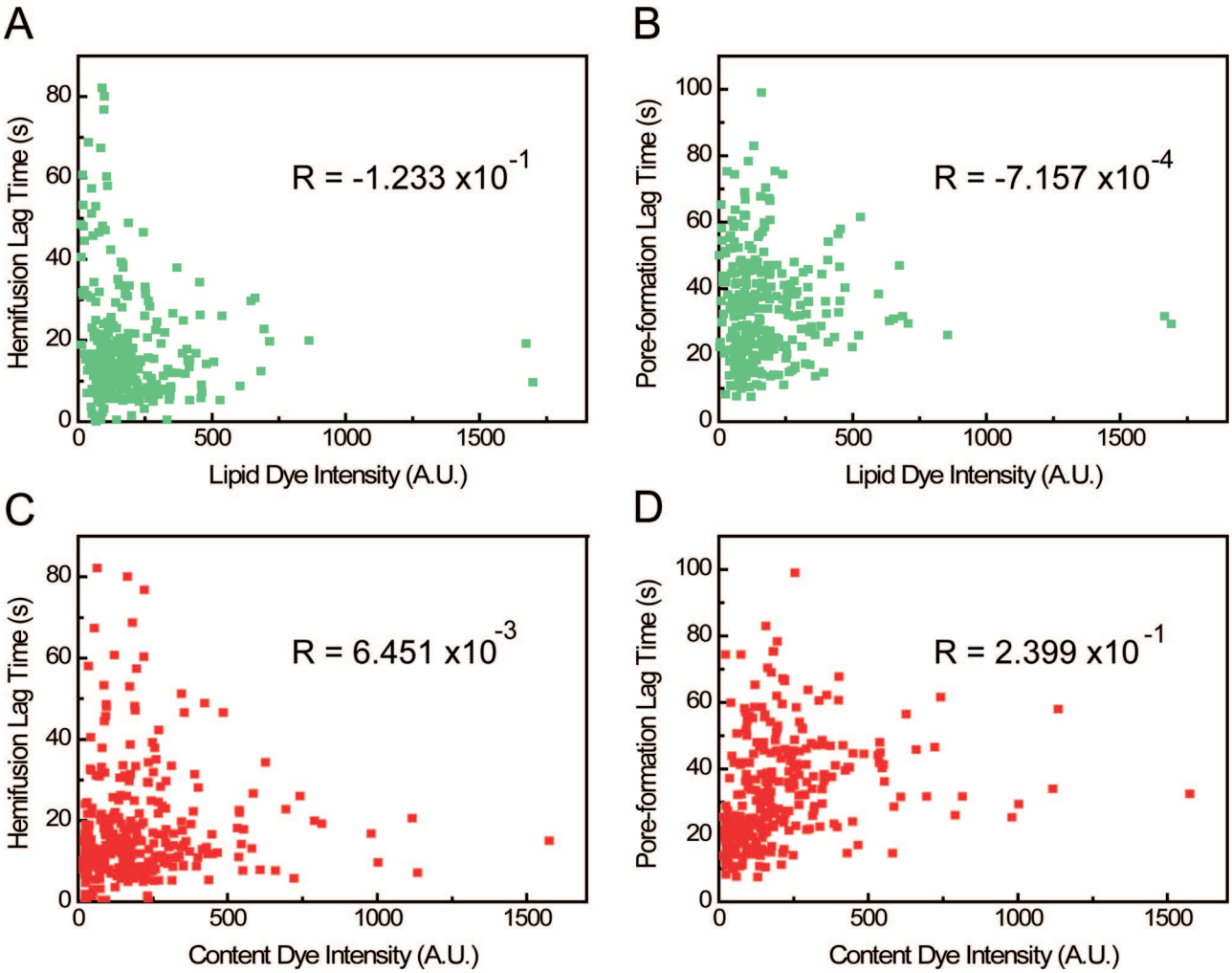

Fig. S2. Scatter plots of the fusion lag times of the particles from Fig. 3*A* as a function of fluorescent dye intensity from individual virus particles. Hemifusion and pore-formation times are plotted as a function of green (lipid) dye intensity (*A* and *B*) and red (content) dye intensity (*C* and *D*). The correlation coefficient (*R*) for each set of lag time and dye intensity is also shown. The low correlation between lag time and dye intensity indicates that incorporation of fluorescent dyes has little effect on fusion kinetics.

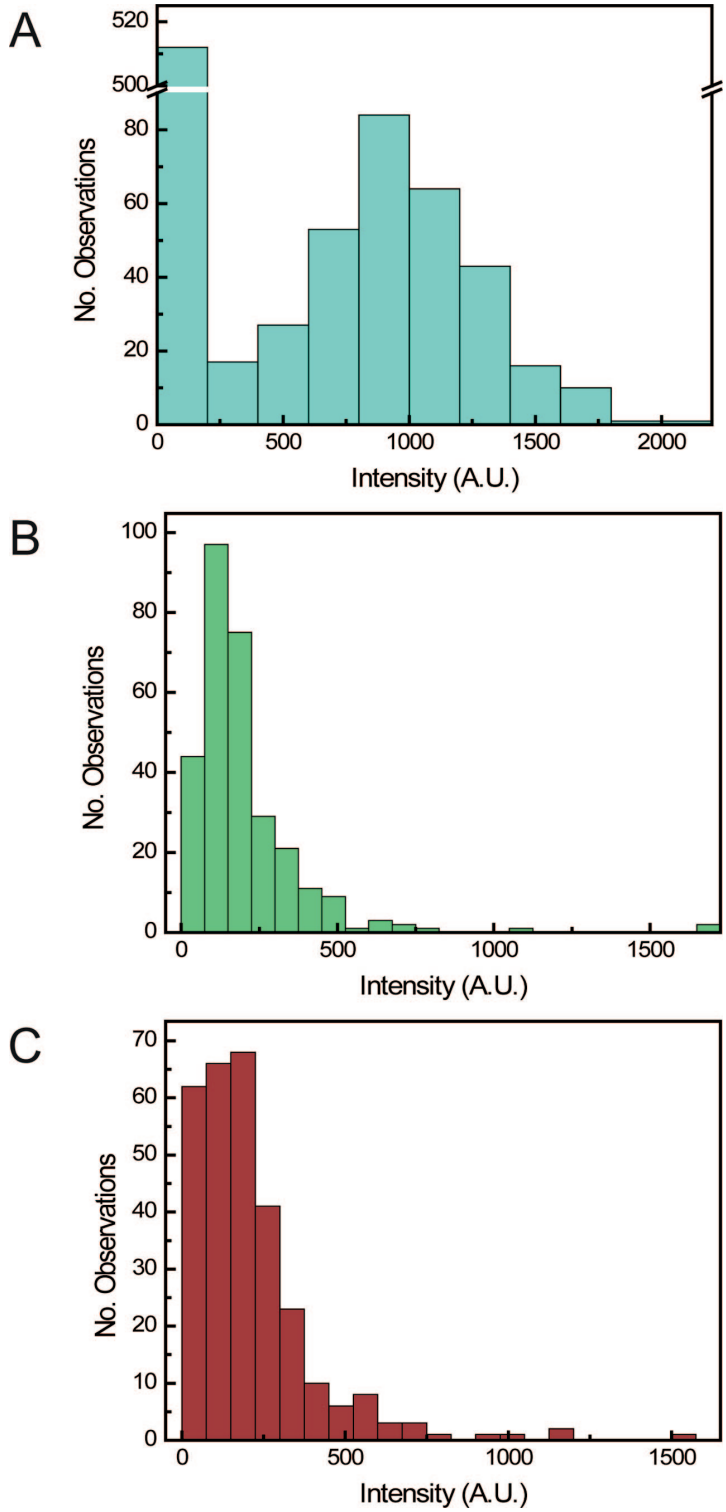

Fig. S3. Distribution of single-particle fluorescence intensities. (*A*) Fluorescence intensity distribution of bilayer-docked virus particles that were covalently coupled to Alexa Fluor 488 trifluorophenyl ester. Labeling was performed according to the manufacturer's instructions (Invitrogen). Although the fluorescent spots are of diffraction-limited size, the unimodal intensity distribution indicates that most of the spots are single virus particles rather than clusters of multiple viruses. The high value of the bar corresponding to the lowest intensities corresponds to individual dye molecules and other background contributions. (*B* and *C*) Distribution of green (Rh110C18; *B*) and red (SRB; *C*) fluorescence intensities from labeled virus particles before membrane fusion. Similar to *A*, the unimodal nature of the distributions suggests that hemifusion and pore formation events arise from individual particles rather than large aggregates. The particles represented in *B* and *C* are the same whose kinetics are summarized in Fig. 3*A*.

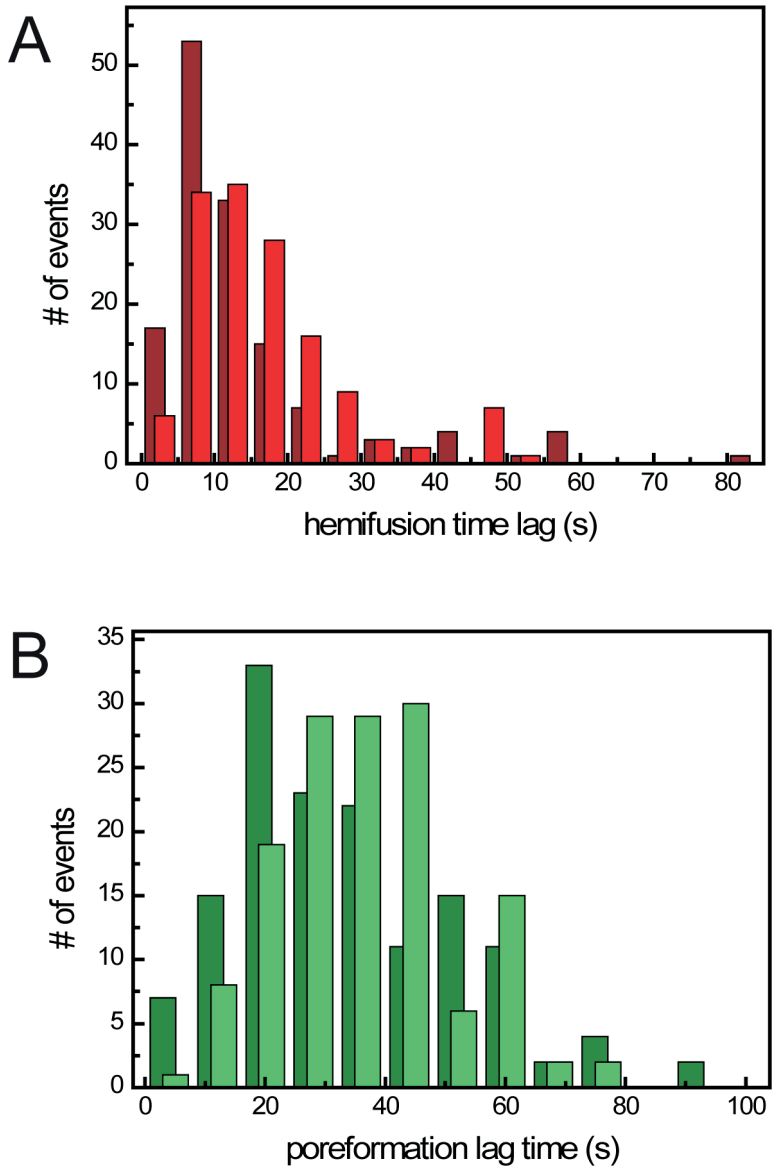

Fig. S4. Effect of the presence of SRB or Rh110C18 on fusion lag-time distributions. (*A*) Distribution of hemifusion lag times in the presence (light red) or absence (dark red) of the content dye SRB. (*B*) Distribution of fusion pore-formation lag times in the presence (light green) or absence (dark green) of the lipophilic dye Rh110C18. Both sets of histograms show complete overlap and indicate that the fluorescent dyes used to detect fusion have little effect on fusion kinetics.

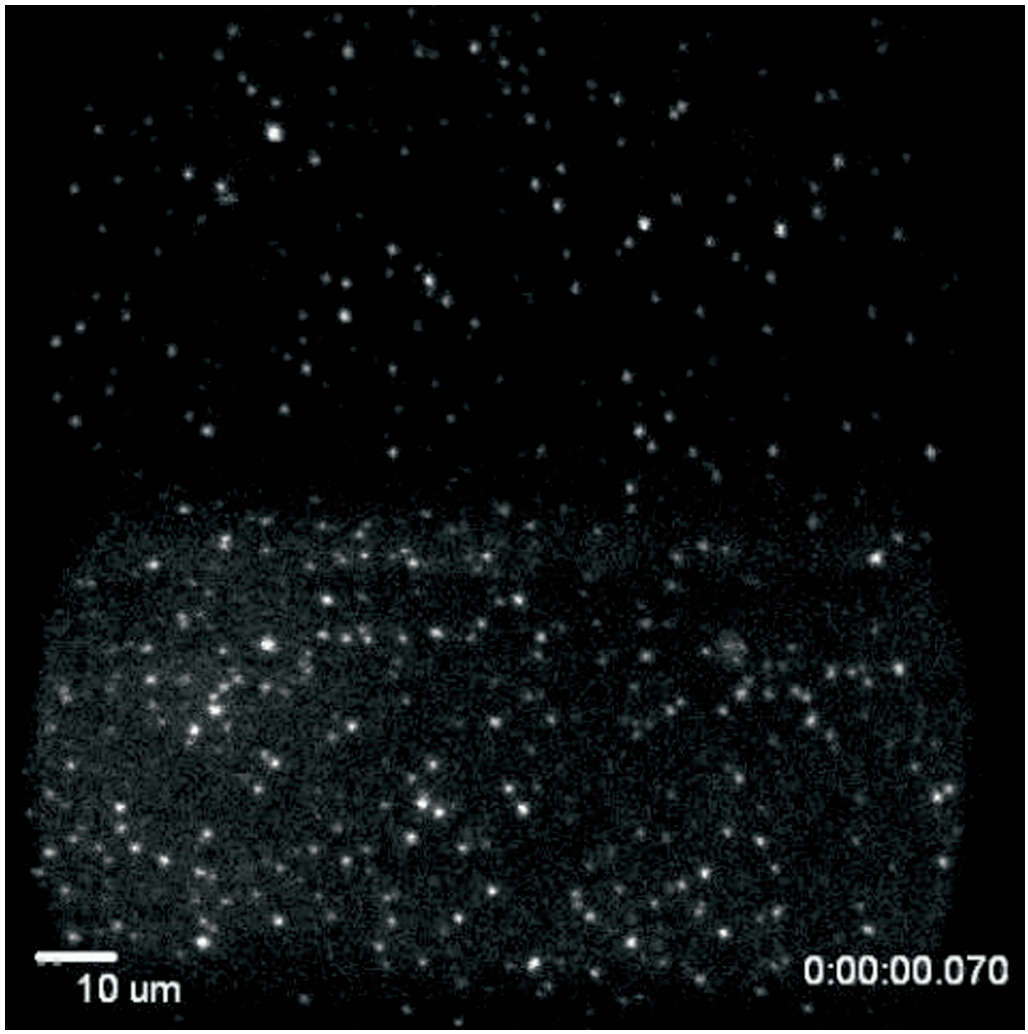

Movie S1. Wide-field fluorescence time-lapsed movie of individual influenza particles fusing with a supported bilayer. *Top* and *Bottom* of the field of view correspond to the red and green fluorescence, respectively, of the same $\sim$70/μm $\times$ 140/μm area of the supported bilayer. Dequenching of the green membrane dye upon hemifusion gives rise to the transient brightening of individual particles (*Bottom*). The sudden decrease of the red fluorescence intensity indicates formation of a fusion pore (*Top*). Acquisition rate is 10 frames per second. Total movie duration corresponds to 61 seconds.

Movie S1